ResearchGate

See discussions, stats, and author profiles for this publication at: https://www.researchgate.net/publication/258801597

Resonance Raman spectroscopic and density functional theory investigation of the excited state structural dynamics of 2-mercapto-1-methylimidazole

ARTICLE *in* JOURNAL OF RAMAN SPECTROSCOPY · APRIL 2013

Impact Factor: 2.67 · DOI: 10.1002/jrs.4238

CITATIONS
7

READS
39

5 AUTHORS, INCLUDING:

Xuming Zheng
Zhejiang Sci-Tech University
109 PUBLICATIONS **1,263** CITATIONS

SEE PROFILE

Available from: Xuming Zheng
Retrieved on: 27 January 2016

Research article

Journal of RAMAN SPECTROSCOPY

Received: 29 July 2012 Revised: 19 November 2012 Accepted: 27 November 2012 Published online in Wiley Online Library: 28 December 2012

(wileyonlinelibrary.com) DOI 10.1002/jrs.4238

Resonance Raman spectroscopic and density functional theory investigation of the excited state structural dynamics of 2-mercapto-1-methylimidazole

Ji-Wen Jian,[a] Hai-Bo Zhang,[a] Cong-Qi Chen,[a] Yanying Zhao[a] and Xuming Zheng[a,b,c]*

The resonance Raman spectroscopy in conjunction with the density functional theory calculations were used to study the excited state structural dynamics of 2-mercapto-1-methylimidazole (MMI). The experimental UV absorption bands were assigned according to the time-dependent density functional calculations. The vibrational assignments were done for the A-band resonance Raman spectra of MMI in water and acetonitrile on the basis of the Fourier transform infrared (FT-IR) and FT-Raman measurements in solid, in water and in acetonitrile and the corresponding B3LYP/6-311+G(d, p) computations. The dynamic structures of MMI were obtained by analysis of the resonance Raman intensity pattern and normal mode analysis. The differences in the dynamic structures of MMI and thiourea were revealed and explained. The structural dynamic of MMI was found to be similar to that of 2-thiopyrimidone in terms of major reaction coordinates and thus favored the intramolecular proton transfer reaction. Copyright © 2012 John Wiley & Sons, Ltd.

Supporting information may be found in the online version of this article.

Keywords: 2-mercapto-1-methylimidazole; excited state; structural dynamics; resonance Raman; density functional theory

Introduction

Thiocarbonyl compounds, in the last two decades, have been a topic among many theoretical and experimental researchers due to its importance in biology, pharmaceutics and fluorescence sensors. The electronic excited state structures,[1–5] decay dynamics[6–9] and solvent effects[10–15] have been reported. The relaxation of the second excited singlet states S_2 ($\pi\pi^*$) was governed by a solvent-dependent non-radiative process.[10,13] Strong chemical interaction was found between the excited states of thione conformer and hydrocarbon solvent in the process of intermolecular photochemistry and photophysics.[11,13] The ground and excited state geometry structures of thiourea, one of the simplest thiocarbonyl compounds, and its derivatives were determined from the theoretical calculations and experimental measurements.[1,16–23] It has been concluded that the geometry structure of thiourea in ground electronic state keeps the coplanarity of N-C(N)=S moiety due to the interaction between the nitrogen lone pairs and the thiocarbonyl π system, while that of thiourea in S_2 ($\pi\pi^*$) excited state undergoes the out-of-plane deformation motion or the pyramidalization of carbon in the N-C(N)=S moiety, and the coplanarity disappears.[23] 2-Mercapto-1-methylimidazole (MMI) is a five-member aromatic heterocyclic derivative of thiourea. Its ground state thiol form (I) → thione form (II) tautomerization reaction (Scheme 1) was previously studied.[24–29] It was revealed that thione (II) dominated in the gas phase and in solution phases on the basis of the infrared (IR),[24] Raman[25] and $^{13}C/^{15}N$ NMR experimental measurements[26,27] and the theoretical computations.[28,29] The crystal structure of MMI in the triclinic system was determined experimentally, and the results also indicated that thione form (II) in dimer, which was formed through the -N-H. . .S=C- hydrogen bonding interaction of two thione form (II), dominated in crystalline state.[24,30–32]

To our knowledge, the electronic excited state structures and dynamics of MMI have not been studied. Resonance Raman spectroscopy in conjunction with density functional theory calculations has been demonstrated to be a powerful tool to obtain above information.[16,33–36] To better understand the excited state behaviors of the five-member aromatic heterocyclic derivatives of thiourea, we reported in this paper, the excited state structural dynamics of MMI in different solvents by using the resonance Raman spectroscopy. The vibrational assignments were done, and the structural dynamics of MMI was obtained. The results were compared to that of thiourea. Significant differences in the excited

* *Correspondence to: Xuming Zheng, Department of Chemistry, Zhejiang Sci-Tech University, Hangzhou 310018, P. R. China. E-mail: zxm@zstu.edu.cn*

a *Department of Chemistry, Zhejiang Sci-Tech University, Hangzhou 310018, P. R. China*

b *Key Laboratory of Advanced Textiles Materials and Manufacture Technology of the Ministry of Education, Zhejiang Sci-Tech University, Hangzhou 310018, P. R. China*

c *Engineering Research Center for Eco-dyeing and Finishing of Textiles of the Ministry of Education, Zhejiang Sci-Tech University, Hangzhou 310018, P. R. China*

Copyright © 2012 John Wiley & Sons, Ltd.

Journal of RAMAN SPECTROSCOPY

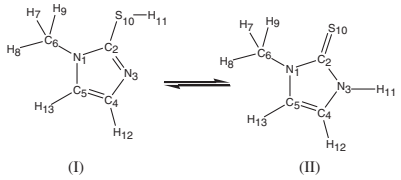

Scheme 1. Thiol (I) → Thione (II) tautomerization of MMI.

state structural dynamics were found between MMI and thiourea, and the underlying mechanism was discussed.

Experimental and computational methods

MMI was purchased from J&K Chemical Company (98% purity, China) and used without purification. The Fourier transform (FT) Raman and FT-IR spectra were obtained using a Thermo Nicolet FT-Raman 960 spectrometer and a Perkin-Elmer1 FT-IR spectrometer with 2 cm^{-1} resolution. The UV absorption spectrum was measured in water and acetonitrile solution using ultraviolet/visible spectrometer.

The resonance Raman experimental methods and apparatus have been described previously,[37–40] so only a short description will be provided here. The harmonics of a nanosecond Nd: YAG laser and their hydrogen Raman shifted laser lines were employed to generate the 239.5, 252.7, 266.0 and 273.9 nm excitation wavelengths utilized in the resonance Raman experiments. The solution phase samples used concentrations of approximately~6.0×10^{-3} mol·l^{-1} MMI (98% purity) in water and in spectroscopic grade acetonitrile (99.5 % purity) solvent. The excitation laser beam used a ~100 μJ pulse energy loosely focused to a 0.5–1.0 mm diameter spot size onto a flowing liquid stream of sample to excite the sample. A backscattering geometry was employed to excite a flowing liquid jet of sample and collect the Raman scattered light with reflective optics that imaged the light through a polarizer and entrance slit of a 0.5 m spectrograph. The grating of the spectrograph dispersed the Raman scattering light onto a liquid nitrogen-cooled charge coupled device detector. The Raman signal was collected for about 90–120 s before being read out to an interfaced PC computer, and 30–40 of these readouts were added together to get the resonance Raman spectrum. The Raman shifts of the resonance Raman spectra were calibrated with the known vibrational frequencies of the cyclohexane solvent Raman bands, and the solvent Raman bands were then subtracted from the resonance Raman spectra by utilizing an appropriately scaled solvent spectrum. Sections of the resonance Raman spectra were fit to a baseline plus a sum of Lorentzian bands to determine the integrated areas of the Raman bands of interest.

The geometry structure optimization and vibrational frequency computation were done using the B3LYP/6-311+G(d,p) level of theory. The S_0—S_n vertical transition energies were estimated at B3LYP-TD/6-311+G(d,p) levels of theory employing a self-consistent reaction field, polarized continuum overlapping spheres model (PCM) and self-consistent isodensity polarizable continuum model (SCIPCM). All of the DFT calculations were done using the Gaussian 09 program.[41]

The excited state gradient at the ground state geometry was calculated using CIS/6-311+G(d,p) and B3LYP-TD(time-dependent density functional theory)/6-311+G(d,p) levels. The relative normal mode displacement Δ_i using the short-time approximation can be given by $\Delta_i = k\omega_i^{-3/2}(\partial V/\partial Q_i)_0$, where $(\partial V/\partial Q_i)_0$ is the derivative of the excited electronic state potential energy surface with respect to the ith normal mode at the ground state geometry and can be computed from projection of the potential energy surface of the excited electronic state at the ground state geometry onto the ith ground state vibrational normal mode.[42,43]

Results and discussion

UV absorption spectra and electronic transitions

Figure 1 shows the UV absorption spectra of MMI in acetonitrile and water with the four excitation wavelengths used for the resonance Raman experiments indicated above the curves. The molar extinction coefficients ε at λ_{max} in acetonitrile and water were measured, respectively, to be 1.701×10^4 l·mol^{-1}·cm^{-1} (at 265 nm), 1.812×10^4 l·mol^{-1}·cm^{-1} (at 251 nm). The λ_{max} blue-shifts about 14 nm in water relative to that in acetonitrile. This suggests that both the polarity and the hydrogen bonding interaction of water play considerable role in modulating the electronic transition energies of MMI in water solution. We have carried out the B3LYP-TD/6-311+G (d, p) level of theory calculations employing PCM and SCIPCM solvent model to assign the UV spectra of MMI and to estimate the solvent effect. Table 1 lists the computed electronic transition energies and the oscillator strengths of MMI in acetonitrile and water. Ten frontier molecular orbitals associated with the electronic transitions of MMI in acetonitrile are briefly summarized in Fig. 2. It shows the highest occupied molecular orbital 30 (HOMO) is a π-type orbital with the major electronic density localized on the ring and sulfur atom. The second highest occupied MO 29 (HOMO-1) is an n-type orbital assignable to the lone pair of the sulfur atom (n_S). The lowest-lying unoccupied MO 31 (LUMO) is an anti-bonding π* orbital with the major electronic density localized on the ring. The second lowest-lying unoccupied MO 32 (LUMO+1) is a π* orbital but with the major electronic density localized on the ring and sulfur atom. The remaining six lowest-lying unoccupied MOs are, respectively, diffuse orbitals, and they are designated as Ryd_1 to Ryd_6. The frontier molecular orbitals associated with the electronic transitions of MMI in solvents of acetonictrile and water are also characterized in similar way. Two most intense experimental bands at 265 nm and 217 nm in acetonitrile or at 251 nm and 212 nm in water are, respectively, assigned as the π→π* transition and n→Ryd/π→π* transitions.

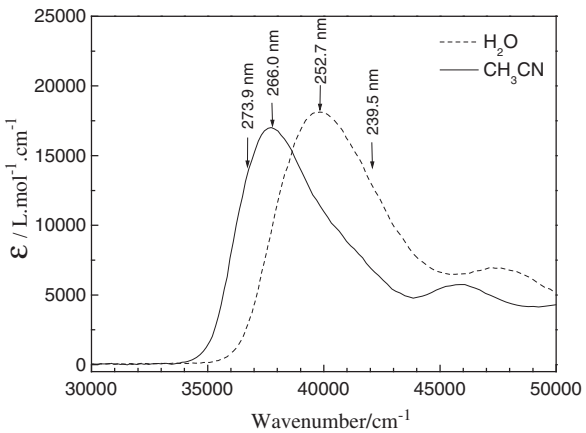

Figure 1. UV absorption spectra of MMI in acetonitrile and water with the four excitation wavelengths used for the resonance Raman experiments indicated.

 Copyright © 2012 John Wiley & Sons, Ltd.

Table 1. B3LYP-TD/6-311+G(d, p) computed electronically singlet transition energy of MMI in acetonitrile and water employing PCM solvent model

	Transition Energy (nm)□		Electronic Transition	Oscillator strength(*f*)		Orbitals (coefficient)
States	Calc.	Expt.		Calc.	Expt.	
in acetonitrile						
$S_1(1^1A")$	261		n→π*	0.0006		29→31(0.705)
$S_2(2^1A")$	254		π→ Ryd_1	0.0713		30→32(0.701)
$S_3(1\ ^1A')$	**251**	**265**	**π→π***	**0.4093**		**30→31(0.692)**
$S_4(2\ ^1A')$	232		n→Ryd_1/π→π*	0.0052		29→32(0.346)/30→33(0.600)
$S_5(3^1A")$	230		π→ Ryd_2/π→Ryd_3	0.0083		30→34(0.672)/30→35(0.189)
$S_6(3\ ^1A')$	228	217	n→Ryd_1/n→Ryd_3	0.1376		29→32(0.592)/29→35(−0.114)
			π→π*			30→33(−0.352)
in water						
$S_1(1^1A")$	260		n→π*	0.0006		29→31 (0.705)
$S_2(2^1A")$	253		π→ Ryd_1	0.0723		30→32(0.701)
$S_3(1^1A')$	**251**	**251**	**π→π***	**0.4080**		**30→31 (0.692)**
$S_4(2^1A')$	231		n→Ryd_1/π→π*	0.0034		29→32 (0.372)/30→33(0.584)
$S_5(3^1A")$	229		π→ Ryd_2/π→Ryd_3	0.0074		30→34 (0.675)/30→35 (0.178)
$S_6(3^1A')$	228	212	n→Ryd_1/n→Ryd_3	0.1403		29→32(0. 576)/29→35(−0.106)
			π→π*			30→33(−0.378)

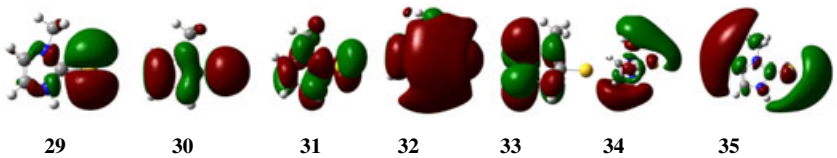

Figure 2. Molecular orbitals associated the electronic transitions (in Table 1) of MMI in acetonitrile.

Vibrational assignments

The vibrational assignments of thiol form (I) of MMI were recently done by Balachandran *et al.*[44] We have carried out the vibrational assignments for thione form (II) of MMI since it dominates in the ground electronic state.[28–32] Figure S1 (Supporting Information) displays the experimental FT-IR and FT-Raman spectra of MMI in solid state. Figures 3 and 4 display, respectively, the experimental FT-Raman spectra of MMI in acetonitrile and water and their comparison to the calculated Raman spectra of thiol form (I) and thione form (II). Table 2 and Table S1 (Supporting Information) list the experimental Raman frequencies of MMI in solid phase as well as in acetonitrile and water. To help assign the experimental vibrational spectra of MMI in solutions, the B3LYP/6-311+G(d, p) calculated Raman frequencies employing PCM solvent model for MMI in water and acetonitrile are also included in Table S1 (Supporting Information).

Comparison of the experiment FT-Raman spectra in solid, acetonitrile and water with the corresponding B3LYP/6-311+G(d, p) calculated Raman spectra of thiol form (I), thione form (II) and the hydrogen-bonded thione dimer reveals that the experimental FT-Raman spectrum of MMI fits in intensity pattern and in

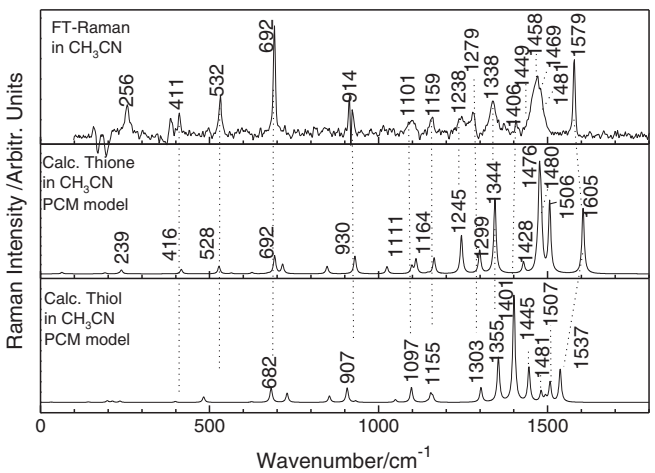

Figure 3. Experimental FT-Raman (top) and calculated Raman spectra of thione form (II) (middle) and thiol form (I) (bottom) in acetonitrile.

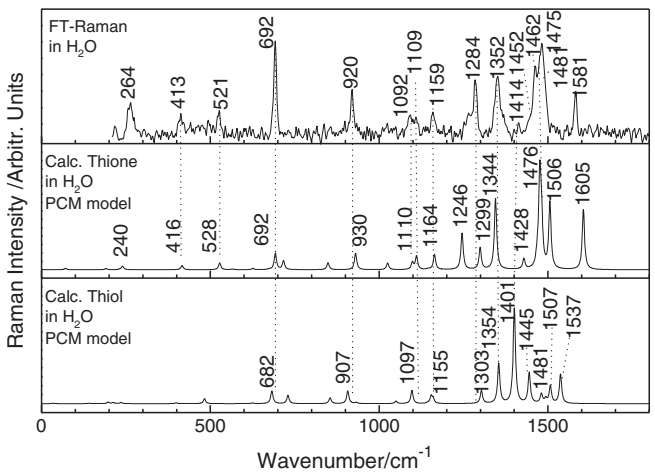

Figure 4. Experimental FT-Raman (top) and calculated Raman spectra of thione form (II) (middle) and thiol form (I) (bottom) in water.

Copyright © 2012 John Wiley & Sons, Ltd.

Table 2. B3LYP/6-311+G(d,p) calculated (in gas phase) and experimental FT-IR and FT-Raman vibrational frequencies and the normal mode descriptions of MMI

		Calculation freq (cm^{-1})			*Experiment*		
Sym Cs	*Modes*	[a]	[b]	[c]	FT-Raman	FT-IR	Descriptions (PED%)
A′	u_1	3669	3603	90.0/81.4	-		ν_{N3H11}(99)
	u_2	3291	3232	0.2/153.5	-	-	ν_{C4H12}(46)+ν_{C5H13}(33) sym
	u_3	3270	3211	3.2/61.0	3162 w	3161 w	ν_{C4H12}(33)+ν_{C5H13}(45) asym
	u_4	3139	3083	8.5/51.3	3106 w	3107 w	ν_{C6H8}(44)+ν_{C6H7}(17)+ν_{C6H9}(17)
	u_5	3047	2993	29.8/149.3	2942 w		ν_{C6H7}(33)+ν_{C6H9}(33)+ν_{C6H8}(25)
	u_6	1607	1580	16.3/75.2	1573 s	1572 s	ν_{C4C5}(90)
	u_7	1521	1496	136.2/28.2	-	-	$\rho_{s\ H7C6H9}$ (61) + δ_{C6H8}(17)
	u_8	1487	1462	164.3/38.7	1465 s	1464 s	$\rho_{s\ H7C6H9}$ (42) + δ_{N3H11}(29)
	u_9	1472	1448	62.1/0.9	1450 wsh	1446 wsh	$\rho_{w\ H7C6H9}\backslash\delta_{C6H8}$(49)+$\nu_{C2N3}$(16)
	u_{10}	1429	1405	32.7/6.8	1406 w	1400 w	methyl umbrella(43) + $\delta_{N3H11}\backslash\delta_{C4H12}\backslash\delta_{C5H13}$(32)
	u_{11}	1330	1308	48.5/28.3	1338 s	1336 m	$\rho_{w\ H7C6H9}\backslash\delta_{C6H8}$(41)+$\nu_{C2N1}$(22) + δ_{N3H11}(13)
	u_{12}	1301	1280	43.9/7.7	1276 s	1275 s	ν_{C6N1}(29) + $\delta_{C4H12}\backslash\delta_{C5H13}$(43)
	u_{13}	1226	1206	58.7/5.1	1253 s	1246 m	ν_{C2N3}(42) + $\delta_{N3H11}\backslash\delta_{C4H12}\backslash\delta_{C5H13}$(50)
	u_{14}	1175	1156	36.6/11.5	1149 w	1149 m	ν_{C2S10}(28) + δ_{C6H8}(27) + $\delta_{C4H12}\backslash\delta_{C5H13}$(27)
	u_{15}	1107	1090	22.8/8.8	1093 m	1093 m	ν_{C4N3}(35) + $\delta_{N3H11}\backslash\delta_{C5H13}$(46)
	u_{16}	1099	1082	10.2/2.8	-	1086 wsh	$\rho_{w\ H7C6H9}\backslash\delta_{C6H8}$(40) + $\delta_{N3H11}\backslash\delta_{C4H12}\backslash\delta_{C5H13}$(41)
	u_{17}	1021	1005	19.1/4.9	1014 w	1014 w	$\rho_{w\ H7C6H9}\backslash\delta_{C6H8}$(33) + $\delta_{N3H11}\backslash\delta_{C4H12}$(31)+$\nu_{C5N1}$(14)
	u_{18}	926	912	3.1/9.6	914 m	914 w	ring deform (98)
	u_{19}	697	687	5.2/15.1	692 s	690 w	ν_{C6N1}(91)
	u_{20}	543	536	12.9/10.7	530 s	530 m	ν_{C2S10}(54) + δ_{C6N1}(32)
	u_{21}	417	413	3.4/3.0	409 w	411 w	δ_{C6N1}(49) + δ_{C2S10}(33)
	u_{22}	243	242	3.6/3.4	264 w	-	δ_{C6N1}(45) + δ_{C2S10}(37)
A″	u_{23}	3111	3055	10.0/47.9	-	3019 w	ν_{C6H7}(37)+ν_{C6H9}(37) asym
	u_{24}	1471	1447	13.3/8.8	-		$\rho_{tH7C6H9}\backslash\gamma_{C6H8}$(95)
	u_{25}	1148	1130	0.1/1.0	-	-	$\rho_{tH7C6H9}\backslash\gamma_{C6H8}$(82)
	u_{26}	824	812	0.6/4.6	850 w	852 w	$\gamma_{C4H12}\backslash\gamma_{C5H13}$(90)
	u_{27}	699	689	69.9/4.2	680 wsh	677 m	$\gamma_{N3H11}\backslash\gamma_{C4H12}\backslash\gamma_{C5H13}$(87)
	u_{28}	663	654	34.3/0.6			$\gamma_{C4H12}\backslash\gamma_{C5H13}$(44) + $\gamma_{N1\text{-}C2\text{-}N3}$(40)
	u_{29}	614	606	4.5/0.8	602 w	602 w	$\gamma_{N3H11}\backslash\gamma_{C4H12}\backslash\gamma_{C5H13}$(54)
	u_{30}	516	510	46/1.7	-		γ_{N3H11}(67) + γ_{C5H13}(11)
	u_{31}	213	213	3.4/0.2		-	Butterfly(65)
	u_{32}	188	188	2.8/0.4		-	γ_{C6N1}(71)
	u_{33}	43	46	0.1/0.9	-	-	$\gamma_{C6H7}\backslash\gamma_{C6H8}\backslash\gamma_{C6H9}$(88)

[a]: Calc = B3LYP/6-311 + (d, p) calculated;

[b]: Calc × 0.98097 + 3.60898;

[c]: Calculated IR/Raman activities; ν=stretch, ρ_s = scissor, ρ_t = twist, ρ_w = wag, δ = in-plane bend, γ = out-of-plane bend; sym. = symmetric, asym. = asymmetric, deform. = deformation; PED: potential energy distribution, only contributions larger than 10% were given s = strong; m = medium; w = weak; wsh = weak shoulder

vibrational frequencies well with the calculated Raman spectrum of thione form (II) but not with that of thiol form (I) for MMI within the 0–2000 cm^{-1} spectral region. This supports the previous prediction that thione form (II) is the predominant component in thione-thiol tautomeric equilibrium.[45–47] Significant discrepancy is noted in the 692 cm^{-1} band intensity between the experimental FT-Raman spectrum and the calculated ones. We have tried PCM and CPCM solvent models and different density function theories, but the predicted Raman spectra are similar. We have also tried 1:1 and 1:2 MMI-H_2O clusters by introducing hydrogen bonding interaction between MMI and H_2O, but it does not noticeably improve the fitness. These results might suggest that more sophisticated theoretic calculation methods are required to address the abnormal 692 cm^{-1} band intensity of thione form (II). Therefore, in this paper we use the frequency consistency to assign the vibrational spectra for MMI.

The correlation of the experimental FT-Raman spectrum of MMI in acetonitrile (Fig. 3) to the calculated one is done. In 0–1000 cm^{-1} region, the experimental FT-Raman spectrum in acetonitrile displays five Raman bands at 256, 411, 532, 692 and 914 cm^{-1}. They correlate well with the calculated Raman bands at 239, 416, 528, 692 and 930 cm^{-1}, respectively, and thus are assigned as ν_{22}, ν_{21}, ν_{20}, ν_{19}, ν_{18}. Similarly, in 1000–1400 cm^{-1} region, five experimental Raman bands at 1101, 1159, 1238, 1279 and 1338 cm^{-1} can correlate well with the calculated Raman bands at 1111, 1164, 1245, 1299 and 1344 cm^{-1}, and are assigned as ν_{16}–ν_{11}. In 1400–1700 cm^{-1} region, a broad experimental band at 1469 cm^{-1} is tentatively deconvolved into four bands at 1449, 1458, 1469 (strong) and 1481 cm^{-1} (Fig. S2 (Supporting Information)). Among them, the 1449 cm^{-1} band is assigned as ν_{24} (A″), while 1458, 1469 and 1481 cm^{-1} bands correlate, respectively, to the calculated bands at 1468 cm^{-1} (ν_9),

Copyright © 2012 John Wiley & Sons, Ltd.

1476 (ν_8) and 1481 cm^{-1} (ν_7). A well-separated experimental band at 1579 cm^{-1} is assigned as ν_6.

The correlation of the experimental FT-Raman spectrum (Fig. 4) of MMI to the calculated one in water is also done. Figures 3 and 4 show that the experimental FT-Raman spectrum of MMI in acetonitrile is in intensity pattern and in vibrational frequencies similar to that in water except for the bands at 1238 and 1469 cm^{-1}. The band at 1238 cm^{-1} is active in acetonitrile and also in solid phase (see also Fig. S1 (Supporting Information) and Fig. 3) but disappears in water. This indicates that it is sensitive to environment. The broad strong band at 1469 cm^{-1} is split into two bands at 1462 and 1481 cm^{-1} in water (Fig. 4) with the 1481 cm^{-1} band being more intense than the 1462 cm^{-1} band. Thus, the bands at 1462 and 1481 cm^{-1} correlate, respectively, to the calculated bands at 1476 cm^{-1} (ν_9) and 1506 cm^{-1} (ν_7), while a shoulder at 1475 cm^{-1} is assigned as ν_8. Further comparison of the FT-Raman spectra of MMI in solid phase to those in acetonitrile and water indicates that they are in intensity pattern and in vibrational frequencies very similar to one another within the 0–2000 cm^{-1} spectral region. Since the agreement between the experimental vibrational frequencies and the calculated ones are in general good for MMI, the normal mode analysis is carried out, and the detailed vibrational assignments as well as the normal mode descriptions for the fundamental modes of MMI are included in Table 2.

Resonance Raman spectra

We have obtained the resonance Raman spectra of MMI in water and acetonitrile at several laser excitations that cover mostly the first intense band (A-band) absorption (λ_{max} = 251 nm in water and λ_{max} = 265 nm in acetonitrile) of MMI. Figure S3 (Supporting Information) displays the overall view of the resonance Raman spectra in acetonitrile and in water. Figure 5 displays the expanded view of the 252.7 nm resonance Raman spectrum of MMI in water (bottom) and 266 nm resonance Raman spectrum of MMI in acetonitrile (top) with the tentative assignments to the larger Raman band features indicated. Since the intensity of some Raman bands in the spectrum may have contributions from several Raman bands that have very close Raman shifts due to limited resolution of the solution phase spectra, the Raman band labels in Fig. 5 only give the largest Raman band contributions to each Raman feature.

Most of the resonance Raman intensity of the 252.7 nm resonance Raman spectrum in water can be assigned to the fundamentals, overtones and combination bands of nine Franck–Condon active vibrational modes: the $H_7C_6H_9$ scissor + N_3-H_{11} in-plane bend (ν_8, 1471 cm^{-1}), CH_3 umbrella +N_3-H_{11}/C_4-H_{12}/C_5-H_{13} in-plane bend (ν_{10}, 1408 cm^{-1}), C_2=N_1 stretch+N_3-H_{11}/C_6-H_8 in-plane bend +$H_7C_6H_9$ wag (ν_{11}, 1353 cm^{-1}), C_6-N_1 stretch +C_4-H_{12}/C_5-H_{13} in-plane bend (ν_{12}, 1280 cm^{-1}), C_2=S_{10} stretch +C_6-H_8/C_4-H_{12}/C_5-H_{13} in-plane bend (ν_{14}, 1185 cm^{-1}), C_4=N_3 stretch +N_3-H_{11}/C_5-H_{13} in-plane bend (ν_{15}, 1102 cm^{-1}), C_4=N_3 stretch+N_3-H_{11}/C_4-H_{12}/C_6-H_8 in-plane bend+$H_7C_6H_9$ wag (ν_{17}, 1019 cm^{-1}), ring deformation (ν_{18}, 917 cm^{-1}), C_6-N_1 stretch (ν_{19}, 689 cm^{-1}). The ν_8, ν_{11}, ν_{12}, ν_{18}, ν_{19} and their overtones and combination bands with other modes dominate the A-band resonance Raman spectrum in water.

Most of the resonance Raman intensity of the 266 nm resonance Raman spectrum in acetonitrile can be assigned to the fundamentals, overtones and combination bands of ten Franck–Condon active vibrational modes: ν_8 (1467 cm^{-1}), ν_{10} (1398 cm^{-1}), ν_{11} (1341 cm^{-1}), ν_{12} (1276 cm^{-1}), C_2=N_3 stretch +N_3-H_{11}/C_4-H_{12}/C_5-H_{13} in-plane bend ν_{13} (1239 cm^{-1}), ν_{14} (1165 cm^{-1}), ν_{15} (1095 cm^{-1}), ν_{17} (1013 cm^{-1}), ν_{18} (926 cm^{-1}), ν_{19} (687 cm^{-1}). The ν_{18}, ν_8, ν_{11}, ν_{19} and their overtones and combination bands with other modes dominate the A-band resonance Raman spectrum in acetonitrile. It appears that the Franck–Condon region structural dynamics of MMI in acetonitrile solvent have significant multidimensional character, predominantly in ν_{18}, ν_{19} and accompanied by moderate contributions from ν_8, ν_{11} and ν_{17} and minor contributions from the remaining six normal modes.

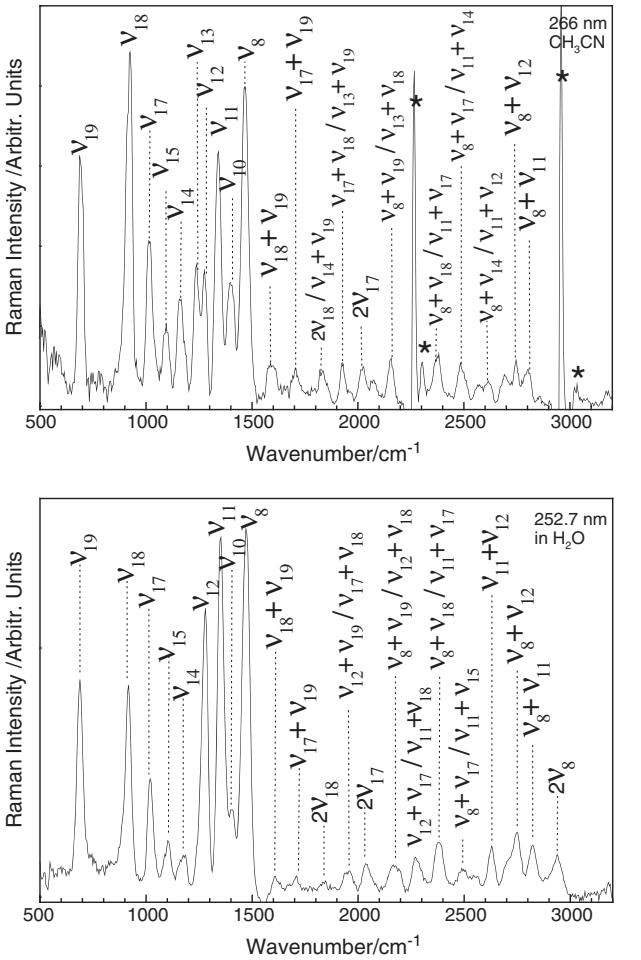

Figure 5. Expanded view of the resonance Raman spectra of MMI in acetonitrile (Top) and in water (Bottom). The spectrum has been intensity corrected and solvent subtracted. Asterisks label parts of the spectrum where solvent subtraction artifacts are present.

Excited state structural dynamics of MMI and comparison to thiourea and 2-thiopyrimidone (2TPM)

Thiourea is a typical aliphatic thiocarbonyl compound, while MMI is a simple aromatic heterocyclic derivative of thiourea. Comparison of the structural dynamics of MMI with that of thiourea[23] in the corresponding $^1\pi\pi^*$ states, as shown in Fig. 6, reveals interesting differences. First, our previous study indicates that the $^1\pi\pi^*$ or S_2 ($2\,^1A$) state of thiourea is not only strongly twisted, but also pyramidalized about the carbon of C=C or C=S group. The geometry distortion and the pyramidalization of carbon atom of thiourea in S_2($2\,^1A$) state is mostly due to the motions of the nontotally symmetric S=C(−N)$_2$ out-of-plane deformation, the totally

Copyright © 2012 John Wiley & Sons, Ltd.

Journal of RAMAN SPECTROSCOPY

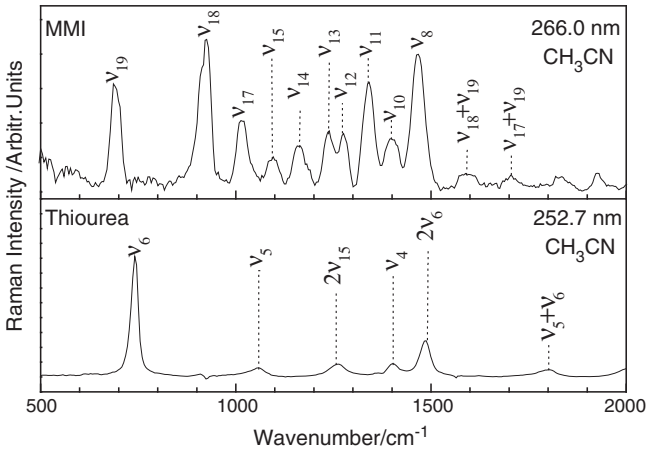

Figure 6. The 266 nm resonance Raman spectra of MMI in acetonitrile (Top) and the 252.7 nm resonance Raman spectra of thiourea in water (Bottom).

symmetric C=S stretch and other vibrational modes in Franck–Condon region. The localized $\pi_{C=S}$ (orbital 19)→$\pi^*_{C=S}$ (orbital 21) transition of thiourea causes, respectively, the sulfur atom and the carbon atom to decrease and increase its electronic density. The net result is that carbon atom tends to have hybrid sp^3 orbital in S_2 state that leads to the pyramidalization of carbon center in the S=C $(-N)_2$ group. However, the resonance Raman spectra of MMI indicate that structural dynamics of MMI is mostly along the in-plane vibrational motions but not along the out-of-plane vibrational motions. This demonstrates that no noticeable pyramidalization of the carbon of C=S group occurs for MMI in Franck–Condon region. This is certainly because of the delocalized π (orbital 30)→π* (orbital 31) transition of MMI, where two π and π* orbitals are delocalized into the whole molecular frame. It appears that the very strong π conjugation of C=S group with the aromatic heterocyclic ring retards the pyramidalization of the carbon of C=S group for MMI.

Examination of Fig. S3 (Supporting Information) and Fig. 5 reveals that the relative intensities of vibtaional modes ν_8 (1462 cm^{-1}) and ν_{11} (1308 cm^{-1}) *versus* ν_{18} (912 cm^{-1}) and ν_{19} (687 cm^{-1}) vary when the solvent changes from acetonitrile to water. Since they reach the maximum at the 252.7 nm resonance Raman spectrum in water and since the oscillator strength of the 265 nm band (f = 0.4093) is much larger than those for the high-lying excited states, the pre-resonance enhancements of ν_8 and ν_{11} from the high-lying excited states are expected to be limited. This indicates that larger excited state structural changes occur along ν_8 and ν_{11} reaction coordinates for MMI in water than in acetonitrile, while larger excited state structural changes happen along ν_{18} and ν_{19} reaction coordinates for MMI in acetonitrile than in water. Similarly, the excited state structural change along ν_{12} (1280 cm^{-1}) reaction coordinate is greater in water than in acetonitrile as indicated by the corresponding intensities of ν_{12} and its combination band $\nu_{11}+\nu_{12}$, while the excited state structural change along ν_{13} (1246 cm^{-1}) reaction coordinate is greater in acetonitrile than in water. It appears that more structural changes occur along N_3–H_{11},C_2-N_1,C_6-N_1 and the methyl coordinates in water, while more structural changes occur along C_2=N_3, N_3–H_{11},C_6-N_1 and ring coordinates in acetonitrile.

To better understand the resonance Raman intensity patterns and the corresponding underlying structural dynamics of MMI in acetonitrile and in water, we have carried out CIS and TD-B3LYP computations to predict the A-band resonance Raman intensity pattern,[42,43] and the results are shown in Fig. 7. Figure 7 indicates that the CIS calculated spectrum in acetonitrile cannot reproduce the experimental 273.9 nm resonance Raman spectrum very well. This is most likely because the CIS method is not advanced enough to predict properly the electronic correlation for the excited state of MMI. TD-B3LYP method is well known to better predict the electronic correlation. The result for MMI in acetonitrile indicates that the TD-B3LYP calculated relative band intensities of ν_{18}, ν_{11}, ν_{19}, ν_{13}, ν_{17}, ν_{14}, ν_{15}, ν_{10} reproduce reasonably

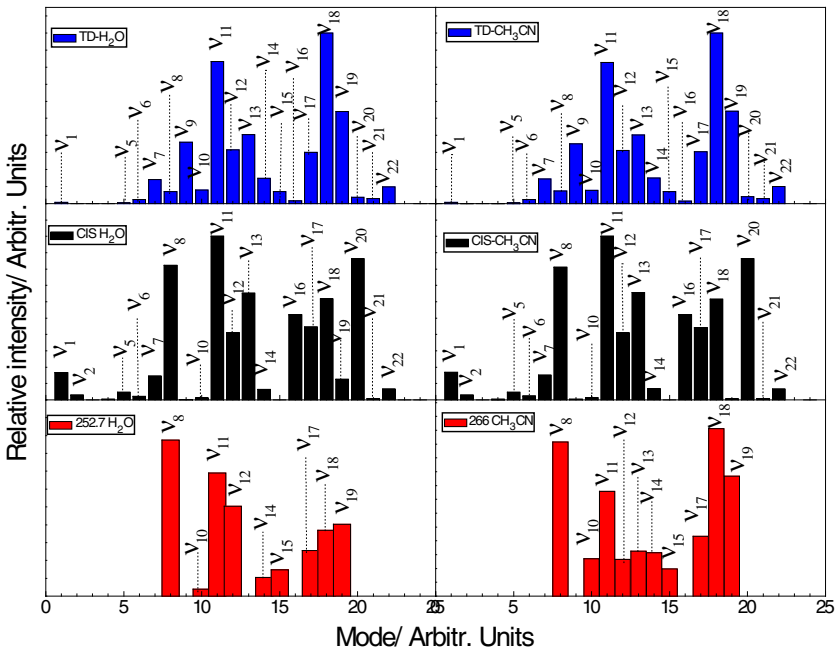

Figure 7. TD-B3LYP (top) and CIS (middle) predicted A-band resonance Raman intensity patterns of MMI in acetonitrile and comparison to the experimental one (bottom).

 Copyright © 2012 John Wiley & Sons, Ltd.

well the corresponding band intensities of the 273.9 nm resonance Raman spectrum. It demonstrates that, in general, TD-B3LYP level of theory can reproduces the major feature of the resonance Raman intensity pattern of MMI in acetonitrile, and this suggests that the Raman process is dominated by the very short time scattering due to solvent-induced damping. Meanwhile, the experimental band intensity of ν_8 is not well fitted by the TD-B3LYP calculated one, and the theoretically predicted minor bands ν_9, ν_7 and ν_{22} are not observed in the experimental spectra, and this demonstrates that certain discrepancy between the TD-B3LYP level of theory prediction and the experimental observation exists still. One possible explanation for it is that the TD-B3LYP level of theory is still not sophisticated enough so that the potential energy surface is not completely predicted. Other possible explanations may be due to the curve-crossings and/or internal conversion, as revealed by our previous resonance Raman and CASSCF studies for several molecular systems. As an example, the structural dynamics of thiophene demonstrates that the S_1/S_3 ($^1B_1/^1A_1$) conical intersection in Franck–Condon region leads to the appearance of the abnormal resonance Raman intensity in the CSC antisymmetry stretch mode ν_{21} (B_2) and ν_{18} (B_2).[48] Therefore, it is possible for MMI that the potential energy surface crossings or internal conversion exist between the interested $^1\pi\pi^*$ excited state and some other dark states (nearly no oscillator strength) of thione form (II) or thiel form (I) in Franck–Condon region, which leads to the activation of new reaction coordinate(s) characteristic to the coupling state, and thus the appearance of some extraordinary resonance Raman band intensities to be unpredictable by TD-B3LYP.

The intra-molecular hydrogen-atom-transfer or electron-transfer coupled proton-transfer process, converting thione form into thiol form, was observed for 2-thiopyridone in water solution[49] and for several matrix-isolated thione compounds, such as 4-thiopyrimidine, 3-thiopyridazine and 2-thiopyridine.[50–52] Hydrogen-atom detachment from the N-H group through the repulsive $\pi\sigma^*$ and/or $n\sigma^*$ states (an electron-transfer coupled proton-transfer process), which takes place in about a hundred femtosecond time-scale, was regarded as a first step of thione → thiol phototautomeric reactions.[50–53] The major available energies for MMI are partitioned into about nine vibrational modes, mostly in the motions of ring deformations, C-H/N_3-H in-plane bends, and the C_2=N_1/C_6-N_1/C_2=S_{10} stretches (as indicated by the normal mode descriptions of ν_{18}, ν_8, ν_{11}, ν_{17}, ν_{19}, ν_{12}, ν_{13}, ν_{14}, etc.). This is very similar to those of 2TPM that also has the major available energies to be partitioned into about nine vibrational modes, mostly in the motions of ring stretches, C-H/N-H in-plane bends, C_4-C_5/C_2=N_1/C_2=S_7 stretches. It appears that the structural dynamics along NH/CH bend reaction coordinates of 2TPM consists with the photoinduced hydrogen atom detachment-attachment or excited state intra-molecular proton transfer (ESIPT) mechanism since the NH/CH bend motions is dynamically required for proton to move from N atom to S atom, and this causes NH/CH bend reaction coordinates to become dynamically active. It seems that the variety of the NH/CH bend reaction coordinates could be served as the marker for hydrogen-detachment-attachment or ESIPT reaction initiated in Franck–Condon region for TPM and its derivatives, as is such for 2-hydroxybenzaldehyde (OHBA) and 2-hydroxyacetophenone (OHAP),[54] in which the ESIPT reactions take play in about a hundred femtosecond time-scale, and the variety of the characteristic C=C-H/C-O-H/C=C-C(=O)/C=C-C(−OH) in-plane bend modes also served as the marker for the ESIPT reaction in the charge-transfer/proton-transfer absorption bands. Therefore, the very similar structural dynamics between MMI and 2TPM in terms of the variety of the CH/NH bend modes characteristic to ESIPT or hydrogen atom detachment-attachment reaction suggests that the initial excited state dynamics of MMI is likely towards the intra-molecular proton transfer reaction.

The excited-state dynamics of MMI differs in water and acetonitrile in that the relative intensities of vibtaional modes ν_8 and ν_{11} *versus* ν_{18} and ν_{19} increase when the solvent changes from acetonitrile to water. This indicates that the salvation and/or hydrogen bonding of water with MMI makes MMI undergo more structural changes along the reaction coordinates of the $H_7C_6H_9$ scissor + N_3-H_{11} in-plane bend mode ν_8, C_2=N_1 stretch+N_3-H_{11}/C_6-H_8 in-plane bend +$H_7C_6H_9$ wag mode ν_{11}, which marks the ESIPT or photoinduced hydrogen detachment-attachment reaction. One possible explanation for it is that the water salvation and/or hydrogen bonding with MMI lowers down the barrier of the excited state tautomerization reaction between thiel form (I) and thione form (II) so that more portion of the excited state wave packet moves along the ν_8 and ν_{11} reaction coordinators towards thiel form (I) photoproduct. This is partially supported by the previous CASSCF and MR-CI calculations that predict a barrier of 18.4 kcal/mol for the similar excited state tautomerization reaction between the 2-hydroxypyridine (2HP) and 2PY monomers in gas phase, which is reduced to 5.6 kcal/mol for the one-water complex and 6.4 kcal/mol for the two water complex.[55] Meanwhile, for MMI in acetonitrile, the motion of excited state wave packet is mainly due to the solvent damping, as Fig. 7 indicated, so that the relative intensities of Franck–Condon active modes reflect mostly the nature of the initial orbital transition, which results in the dominant intensities of the ring deformation mode ν_{18} and C_6-N_1 stretch mode ν_{19} appearing in the spectra.

Conclusion

The structural dynamics of MMI in the S_3(1 ^{1}A′ or $^1\pi\pi^*$) electronic state are studied by using the resonance Raman spectroscopy and density-functional theory computations. The vibrational spectra are assigned, and the normal mode analysis is done. Most of the A-band resonance Raman features of MMI can be assigned to the fundamentals, overtones and combination bands of about nine Franck–Condon active vibrational modes: ν_8, ν_{10}, ν_{11}, ν_{12}, ν_{14}, ν_{15}, ν_{17}, ν_{18}, ν_{19}. Larger excited state structural changes occur along ν_8 and ν_{11} reaction coordinates for MMI in water than in acetonitrile, while larger excited state structural changes happen along ν_{18} and ν_{19} reaction coordinates for MMI in acetonitrile than in water. Moreover, the excited state structural change along ν_{12} reaction coordinate is greater in water than in acetonitrile, while the excited state structural change along ν_{13} reaction coordinate is greater in acetonitrile than in water. It appears that more structural changes occur along N_3–H_{11},C_2-N_1,C_6-N_1 and the methyl coordinates in water, while more structural changes occur along C_2=N_3, N_3–H_{11},C_6-N_1 and ring coordinates in acetonitrile.

Interesting differences in the structural dynamics of MMI and thiourea in the corresponding $^1\pi\pi^*$ states are revealed. Relative to the pyramidalization of carbon atom of thiourea, the coplanarity of the molecular frame is kept, and no pyramidalization of carbon atom is observed for MMI. It appears that the very strong π conjugation of C=S group with the aromatic heterocyclic ring retards the pyramidalization of the carbon of C=S group for MMI. Significant similarities in the structural dynamics of MMI and 2TPM in the corresponding $^1\pi\pi^*$ states are noted. It appears that the structural dynamics along NH/CH bend reaction

Copyright © 2012 John Wiley & Sons, Ltd.

coordinates for MMI and 2TPM correlate with the photoinduced hydrogen-atom detachment-attachment or electron-transfer coupled proton-transfer mechanism.

CIS and TD-B3LYP computations were used to predict the A-band resonance Raman intensity patterns of MMI in acetonitrile and in water. The results demonstrates that, in general, TD-B3LYP level computation can reproduce the major feature of the resonance Raman intensity pattern of MMI in acetonitrile and the Raman process of MMI in acetonitrile is dominated by the very short time scattering due to solvent-induced damping.

Acknowledgements

This work was supported by grants from NNSFC (No.21033002 and No.21273202).

Supporting information

Supporting information may be found in the online version of this article.

References

[1] R. P. Steer, *Rev. Chem. Intermed.* **1981**, *4*, 1.
[2] A. Maciejewski, M. Szymanski, R. P. Steer, *Chem. Phys. Lett.* **1988**, *143*, 6.
[3] A. Maciejewski, M. Szymanski, R. P. Steer, *Chem. Phys.* **1992**, *165*, 101.
[4] L. L. Lu, X. F. Wang, K. Yuan, *J. Mol. Struct. (Theochem).* **2007**, *809*, 73.
[5] H. G. Wang, B. Liu, X. M. Zheng, *J. Raman. Spectros.* **2009**, *40*, 992.
[6] M. Szymanski, A. Maciejewski, *J. Phys. Chem.* **1988**, *92*, 2485.
[7] A. Maciejewski, R. P. Steer, *Chem. Rev.* **1993**, *93*, 67.
[8] A. Maciejewski, M. Szymanski, R. P. Steer, *J. Phys. Chem.* **1986**, *90*, 6314.
[9] S. R. Abrams, R. P. Steer, M. Szymanski, *Chem. Phys. Lett.* **1987**, *139*, 182.
[10] M. Mahaney, J. R. Huber, *Chem. Phys. Lett.* **1984**, *105*, 395.
[11] A. Maciejewski, D. R. Demmer, R. P. Steer, *J. Am. Chem. Soc.* **1985**, *107*, 2831.
[12] A. Maciejewski, M. Szymanski, R. P. Steer, *J. Phys. Chem.* **1988**, *92*, 6939.
[13] A. Maciejewski, R. P. Steer, *Chem. Phys. Lett.* **1983**, *100*, 540.
[14] R. P. Steer, V. Ramamurt, *Acc. Chem. Res.* **1988**, *21*, 380.
[15] M. Szymanski, R. P. Steer, A. Maciejewsk, *Chem. Phys. Lett.* **1987**, *135*, 243.
[16] X. N. Guo, R. Du, Y. Y. Zhao, K. M. Pei, H. G. Wang, X. M. Zheng, *Acta. Phys. Chim. Sin.* **2012**, *28*, 1570.
[17] A. Kapur, R. P. Steer, P. G. Mezey, *J. Chem. Phys.* **1979**, *71*, 588.
[18] C. Fang, G. Z. Wu, *J. Raman Spectros.* **2007**, *38*, 1416.
[19] H. Rostkowska, L. Lapinski, M. J. Nowak, *J. Phys. Chem. A* **2003**, *107*, 6373.
[20] L. Lapinski, H. Rostkowska, M. Yaman, M. J. Nowak, *J. Phys. Chem. A* **2004**, *108*, 5551.
[21] T. Sihiguro, E. I. Suzuki, M. Tsuboi, *J. Mol. Spectros.* **1980**, *83*, 360.
[22] A. T. Kowal. *J. Comput. Chem.* **2011**, *32*, 718.
[23] H. B. Zhang, Y. Y. Zhao, X. M. Zheng, *Chin. J. Chem. Phys.* **2012**, *25*, 1.
[24] H. T. Flakus, A. Miros, P. G. Jones, *Spectrochimica Acta Part A* **2002**, *58*, 225.
[25] P. P. Jesus, G. D. Melchor, H. B. Joaquin, *Collect. Czech. Chem. Comm.* **1989**, *54*, 2045.
[26] R. Fauré, E. J. Vincent, J. Metzger, *Org. Magn. Reson.* **1977**, *9*, 688.
[27] E. B. Olejnik, L. Stefaniak, M. Witanowski, G. A. Webb, *Magn. Reson. Chem.* **1985**, *23*, 166.
[28] Y. Ren, J. Ren, S. Y. Chu. *J. Mol. Struct. (Theochem).* **2005**, *730*, 199.
[29] H. Roohi, S. Baghery, S. G. Hosseini, *Bull. Chem. Soc. Jpn.* **2008**, *81*, 1402.
[30] C. Guimon, G. P. Guillouzo, M. Arbelot, *Tetrahedron* **1974**, *30*, 3831.
[31] E. S. Raper, J. R. Creighton, R. E. Oughtred, *Acta Crystallogr. B* **1983**, *39*, 355.
[32] G. Vampa, S. Benvenuti, F. Severi, *J. Heterocycl. Chem.* **1995**, *32*, 227.
[33] H. G. Wang, W. F. Zhang, B. Liu, X. M. Zheng, *J. Phys. Chem. A* **2011**, *115*, 14282.
[34] B. Liu, J. Xu, X. M. Zheng, H. G. Wang, *J. Raman. Spectros.* **2010**, *41*, 1185.
[35] H. G. Wang, B. Liu, J. M. Wan, X. M. Zheng, *J. Raman. Spectros.* **2009**, *40*, 992.
[36] S. L. Wei, H. G. Wang, X. M. Zheng, *Chem. Phys. Lett.* **2010**, *495*, 222.
[37] X. M. Zhu, S. Q. Zhang, X. M. Zheng, D. L. Phillips, *J. Phys. Chem. A* **2005**, *109*, 3086.
[38] X. M. Zheng, Y. L. Li, D. L. Phillips, *J. Phys. Chem. A* **2004**, *108*, 8032.
[39] K. F. Weng, Y. Shi, X. M. Zheng, D. L. Phillips, *J. Phys. Chem. A* **2006**, *110*, 851.
[40] X. M. Zheng, D. L. Phillips, *J. Chem. Phys.* **1998**, *108*, 5772.
[41] M. J. Frisch, G. W. Trucks, H. B. Schlegel, G. E. Scuseria, M. A. Robb, J. R. Cheeseman, G. Scalmani, V. Barone, B. Mennucci, G. A. Petersson, H. Nakatsuji, M. Caricato, X. Li, H. P. Hratchian, A. F. Izmaylov, J. Bloino, G. Zheng, J. L. Sonnenberg, M. Hada, M. Ehara, K. Toyota, R. Fukuda, J. Hasegawa, M. Ishida, T. Nakajima, Y. Honda, O. Kitao, H. Nakai, T. Vreven, J. A. Montgomery, J. E. Peralta, F. Ogliaro, M. Bearpark, J. J. Heyd, E. Brothers, K. N. Kudin, V. N. Staroverov, R. Kobayashi, J. Normand, K. Raghavachari, A. Rendell, J. C. Burant, S. S. Iyengar, J. Tomasi, M. Cossi, N. Rega, J. M. Millam, M. Klene, J. E. Knox, J. B. Cross, V. Bakken, C. Adamo, J. Jaramillo, R. Gomperts, R. E. Stratmann, O. Yazyev, A. J. Austin, R. Cammi, C. Pomelli, J. W. Ochterski, R. L. Martin, K. Morokuma, V. G. Zakrzewski, G. A. Voth, P. Salvador, J. J. Dannenberg, S. Dapprich, A. D. Daniels, O. Farkas, J. B. Foresman, J. V. Ortiz, J. Cioslowski, D. J. Fox, *Gaussian 09, Revision A.1*, Gaussian, Inc., Wallingford CT, **2009**.
[42] L. M. Markham, B. S. Hudson, *J. Phys. Chem.* **1996**, *100*, 2731.
[43] X. Zheng, C. W. Lee, D. L. Phillips, *J. Chem. Phys.* **1999**, *111*, 11034.
[44] V. Balachandrana, A. Lakshmi, A. Janaki, *J. Mol. Struct.* **2011**, *1006*, 395.
[45] J. G. Contreras, S. T. Madariaga, *J. Phys. Org. Chem.* **2003**, *16*, 47.
[46] A. P. Fu, H. L. Li, D. M. Du, *J. Mol. Struct. (Theochem).* **2006**, *767*, 51.
[47] A. K. Rai, R. Singh, K. N. Singh, V. B. Singh, *Spectrochimica Acta Part A.* **2006**, *63*, 483.
[48] X. F. Wu, X. Zheng, H. G. Wang, Y. Y. Zhao, X. G. Guan, D. L. Phillips, X. B. Chen, W. H. Fang, *J. Chem. Phys.* **2010**, *133*, 134507.
[49] R. Du, C. Liu, X. M. Zheng, D. L. Phillips, *J. Phys. Chem. B* **2011**, *115*, 8266.
[50] M. J. Nowak, L. Lapinski, J. Fulara, A. Les, L. Adamowicz, *J. Phys. Chem.* **1991**, *95*, 2404.
[51] M. J. Nowak, L. Lapinski, H. Rostkowska, A. Les, L. Adamowicz, *J. Phys. Chem.* **1990**, *94*, 7406.
[52] H. Rostkowska, L. Lapinski, M. J. Nowak, *J. Phys. Org. Chem.* **2010**, *23*, 56.
[53] B. Chmura, M. F. Rode, A. L. Sobolewski, L. Lapinski, M. J. Nowak, *J. Phys. Chem. A* **2008**, *112*, 13655.
[54] X. L. Jiang, K. M. Pei, H. G. Wang, X. Zheng, W. H. Fang, D. L. Phillips, *J. Phys. Chem. A* **2007**, *111*, 13182.
[55] Q. S. Li, W. H. Fang, J. G. Yu, *J. Phys. Chem. A* **2005**, *109*, 3983.

Copyright © 2012 John Wiley & Sons, Ltd.